JPRS-JST-93-014
30 MARCH 1993

JPRS Report

Science & Technology

Japan

1992 TRDI CONFERENCE ON MILITARY R&D RESULTS

19980506 045

DTIC QUALITY INSPECTED 2

DISTRIBUTION STATEMENT A
Approved for public release;
Distribution Unlimited

REPRODUCED BY
U.S. DEPARTMENT OF COMMERCE
NATIONAL TECHNICAL INFORMATION SERVICE
SPRINGFIELD, VA 22161

JPRS-JST-93-014
30 MARCH 1993

SCIENCE & TECHNOLOGY
JAPAN

1992 TRDI CONFERENCE ON MILITARY R&D RESULTS

93FE0340 Tokyo TECHNICAL RESEARCH AND DEVELOPMENT INSTITUTE, DEFENSE AGENCY in Japanese Nov 92 p i-24

CONTENTS

1992 TRDI Conference on Military R&D Results

93FE0340A Tokyo TECHNICAL RESEARCH AND DEVELOPMENT INSTITUTE, DEFENSE AGENCY in Japanese Nov 92 pp i-iv

[Text] **Table of Contents**

Time: 10 November 1992 (Tuesday)
Place: TRDI HQ Lecture Hall

-Break-

Moderator: Ronosuke Kubota, Director General of Bureau 2, Third Research Center

-Break-

Moderator: Shinkichi Nishimoto, Director General of Bureau 3, Third Research Center

Time: 10 November 1992 (Tuesday)
Place: TRDI HQ Lecture Hall

Moderator: General Sakamoto, Director General of Bureau 2, Second Research Center

(12) 1650–1720 Sound Absorption of Pine Wedges in Relation to Pressure.....24
Sanao Yamashita, Toshiaki Takahashi
Tomigo Yoroi

1720–1730 Closing Remarks, Director General, Technology Bureau

Estimation of Combustion Temperature of Liquid Propellants Using Spectrometric Methods

93FE0340A Tokyo TECHNICAL RESEARCH AND DEVELOPMENT INSTITUTE, DEFENSE AGENCY in Japanese Nov 92 p 1

[Article by Shiro Kushima and Hideaki Mukai, staff members, Firearms Research Office, Bureau 1, First Research Center, TRDI]

[Text] **1. Objective**

To attempt to estimate the internal temperature of the combustion chamber during injection of liquid propellants by analyzing the spectrum of the combustion flash and measuring the distribution of intensity by wavelength (spectrometric method), and to the results with measurement by conventional radiant temperature measurement.

2. Methods Used and Content

The liquid propellant is injected into a high-temperature, high-pressure environment obtained by combustion of line explosive. The combustion flash after injection is measured by means of the test equipment shown in Figure 1, and the intensity of combustion flash is measured for each wavelength. The combustion temperature is calculated on the assumption that the intensity distribution follows Planck's law.

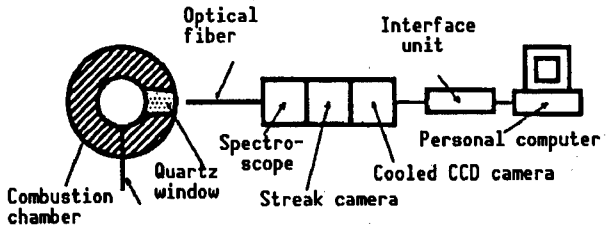

Figure 1. Block Diagram of Test Equipment

3. Results and Observation

(1) Results

The observed data and approximation curve shown in Figure 2 were obtained, and from those were derived the temperature calculations shown in Figure 3. Combustion of propellant is accompanied by chemical luminescence other than the black body radiation; to eliminate the effect of that, data was used only from the wavelengths (490~508 nm and 696~714 nm) where there was little effect from the luminescence, and combustion temperature was estimated using the

least-squares method. That data was then used to find ambient temperature at time of injection of liquid propellant and combustion temperature at time of peak combustion of liquid propellant, as shown in Figure 4.

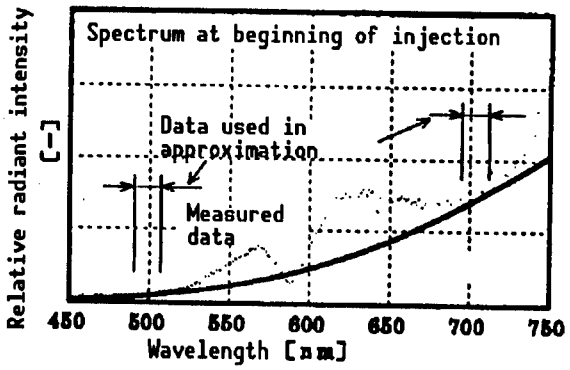

Figure 2. Sample of Measured Data

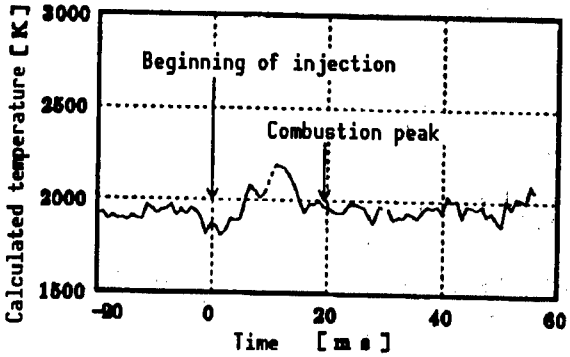

Figure 3. Calculation of Temperatures by Spectrometric Method

(2) Observations

This measurement was calculated with the interior of the combustion chamber regarded as a grey body; judging from the calculated results, that appears to be a correct hypothesis for measurement of high ambient temperatures. Near the time of peak combustion of the liquid propellant, the flash is dominant, and measurement by this formula becomes difficult. Based on test results, the proportion radiated by propellant combustion gases is thought to be 0.08~0.11 between 1800~2100 K.

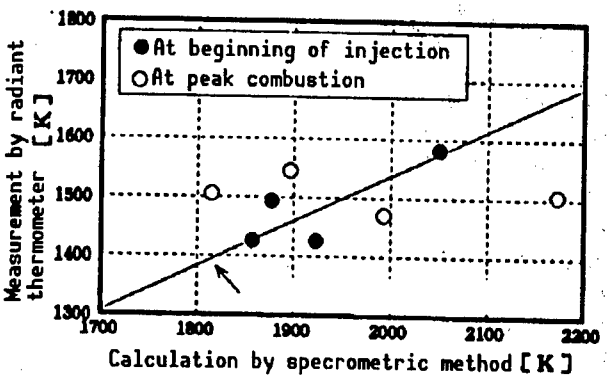

Figure 4. Comparison of Temperatures by Method of Measurement

Stabilized Nitrocellulose, LOVA Propellants

93FE0340B Tokyo TECHNICAL RESEARCH AND DEVELOPMENT INSTITUTE, DEFENSE AGENCY in Japanese Nov 92 p 2

[Article by Haruyuki Arisawa, Junichi Kimura, Toshihiko Shimizu and Tsuneo Koura, staff members, Ammunition Research Office, Bureau 1, First Research Center, TRDI]

[Text] **1. Objective**

Conventional propellants consisting primarily of nitroglycerine and nitrocellulose have good combustion characteristics, but there are problems with their vulnerability to heat and shock; there have been numerous reports of secondary explosions in fires or when hit by a shell on the battlefield. There has been, therefore, strong demand for propellants that have LOVA (low-vulnerability ammunition) properties in addition to conventional properties. The LOVA properties of conventional nitrocellulose propellants have been improved by physically mixing in heat-resistant materials (such as cellulose acetate butylate, CAB). This office has attempted to reduce combustibility chemically by replacing some of the nitrate ester groups in nitrocellulose with less-combustible acetyl groups. The objective of this research has been to fabricate cellulose acetate nitrolate (CAN), investigate the basic properties of CAN by itself and its fundamental sensitivity and combustion properties when formed into a propellant, and to compare it with conventional propellants.

2. Methods Used and Content

The samples used in this research were nitrocellulose (NC) with a nitrogen content of 12.6%, and three varieties of CAN with the degree of acetylation varied from 0.7~2.0, used alone and formed as a propellant by adding such things as RDX. The temperature stability of simple NC and CAN were evaluated using thermogravimetry and differential scanning calorimetry (DSC). The samples formed into propellant underwent tension and compression tests, drop sensitivity tests and sealed bomb tests, and the LOVA properties and combustion properties were compared with a general triple-based propellant (M30A1).

3. Results and Observations

(1) Results

Figure 1 plots, using the Ozawa method, the peak temperature and rate of heating of CAN with a 2.0 degree of acetylation and of NC, as shown by differential scanning calorimetric analysis. The black triangles in the Figure are where it was determined samples ignited, from the exothermic peak. Figure 2 shows the results of drop sensitivity tests of three types of CAN propellant and M30A1 with NC as a binder. Figure 3 shows the pressure index of combustion speed, across a temperature range from -30~50°C, of a propellant with CAN having a 0.6 degree of alkylation as a binder and M30A1 propellant.

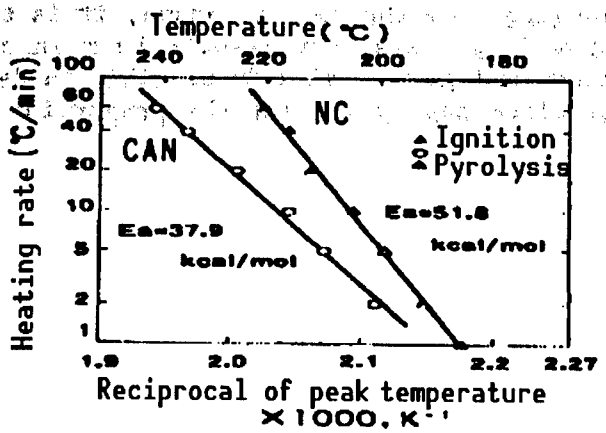

Figure 1. DSC Data for CAN and NC

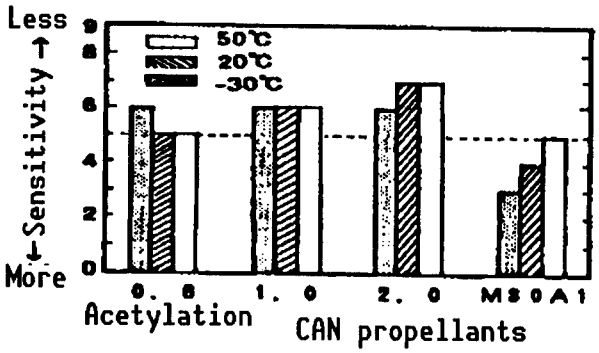

Figure 2. Comparison of Drop Sensitivity in CAN Propellants

(2) Observations

Figure 1 shows that, compared with NC that ignited at heating rates of 20°C and above, CAN did not ignite at the temperatures measures, and had become less combustible than NC. The activation energy of NC is about 52 kcal/mol, but that of CAN is only about 38 kcal/mol, indicating high temperature-resistance when heated at high rates.

Figure 2 confirms that the drop sensitivity of CAN propellants is lower than that of M30A1 propellant, and decreases as alkylation increases. Moreover, because of the relationship between drop sensitivity and firing sensitivity that we reported last time, it can be assumed that CAN has adequate LOVA properties in terms of firing sensitivity as well.

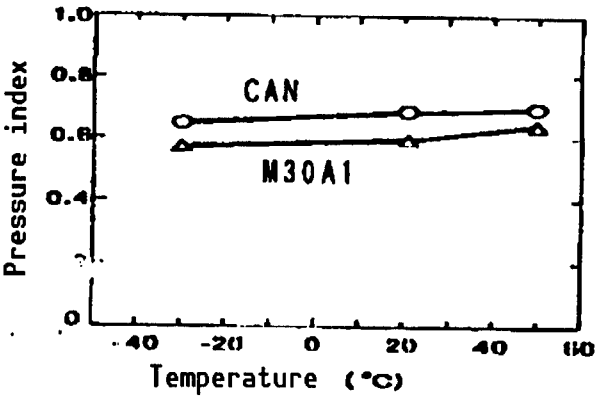

Figure 3. Pressure Index Dependence on Temperature in CAN and M30 Propellants

Figure 3: propellants consisting primarily of conventional nitroamine compounds have problems in terms of combustion properties, because of pressure indices in excess of 1.0. It can be seen from Figure 3, however, that when nitroamine propellants are used with CAN as a binder, the pressure can be suppressed to the same level as M30A1.

Judging from the results above, it is thought that use of CAN as a binder can provide satisfactory results both in combustion properties and LOVA properties, and that it will be possible to developed propellants that meet specific requirements by varying the proportion of alkyl groups within the molecule.

Spallation in Steel (Spallation Damage in Flat Plate Impact Test)

93FE0340C Tokyo TECHNICAL RESEARCH AND DEVELOPMENT INSTITUTE, DEFENSE AGENCY in Japanese Nov 92 p 3

[Article by Toshikatsu Mayama, staff member, Armor Systems Research Office, 2nd Bureau, First Research Center]

[Text] **1. Objective**

The damage phenomenon when shock waves cause cracks in metal materials is called spallation, and the behavior of the damage is known to vary with the material. With the advance of mathematical simulation technology in recent years, however, the spallation behavior for various structures has been explicated by means of numerical calculations, and it has become necessary to induce spallation artificially, inspect the damaged areas and acquire the damage parameters.

For this report, spallation damage cause in flat impact tests received macroscopic and microscopic examination, and the nature of spallation damage was considered.

2. Methods Used and Content

To produce ideal spallation, it is necessary to use a test system that will produce flat shock waves. For that reason, we used a procedure called the flat plate impact test devised in the late 1950s to measure Ugonio properties (see Figure 1). Soft recovery was necessary so that the samples would not be deformed except by the phenomenon under study, so it became necessary to study and improve recovery methods that would minimize deformation.

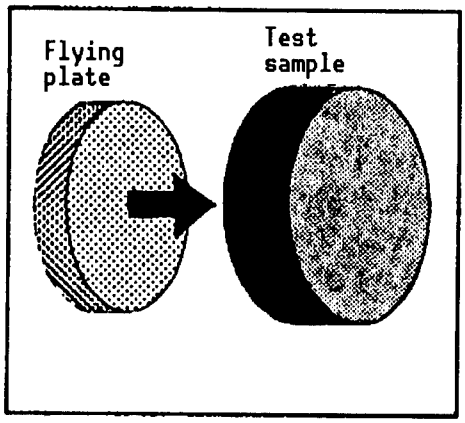

Figure 1. Flat Plate Impact Test

3. Results and Observations

(1) Results

Origin analysis based on earlier soft recovery data was performed, the origins of sample deformation during soft recovery were hypothesized, and counter-measures were devised. Most of the deformation of samples that occurred during soft recovery was prevented as a result, and mutual examination with simulation results could be done easily (see Figure 2 [not reproduced]).

Macroscopic and microscopic examination of the damaged surface and cross section of the damage was done for three materials: SM-41B, SS-41 and rotor material (used for steam turbines). As a result it was determined that exfoliation in the damaged cross section was as great as for materials with low static material strength. The most important result was that while there were numerous cracks in the SM-41B in multiple layers, cracks in SS-41, which is a similar material, was clearly demarcated in one or two layers (see Figure 3 [not reproduced]). Moreover, it was determined through observation at high magnifications that spallation cracking is a matter of connection of very small voids.

(2) Observations

The samples and observation results were all of low-strength materials, but it was possible to obtain useful, basic data about the nature of spallation damage. Various materials will be analyzed hereafter; this is expected to assist in explication of the phenomenon of penetration damage.

Generating Very High Pressure With Shock Wave Convergence

93FE0340D Tokyo TECHNICAL RESEARCH AND DEVELOPMENT INSTITUTE, DEFENSE AGENCY in Japanese Nov 92 p 4

[Article by Hiroshi Kunishige, staff member, 1st Armor Research Office, Bureau 2, First Research Center]

[Text] **1. Objective**

The flying plate impact method, in which gunpowder or explosives are used to make a flying metal plate collide with a target, yields high dynamic pressure, and so has been used in research to decide such things as solid state equations. There are limits, however, to the acceleration of the flying plate by increasing the amount of explosive, and consequently there are limits to the impact pressure that can be obtained. For that reason, there has been research on methods to generate high pressure by convergence of shock waves, as an effective method to obtain high dynamic pressure. For example, in the gun barrel flying plate impact method, we have done experimental research to concentrate shock waves above the central axis of a target with two-layer, cylindrical structure with an outer cylinder of aluminum alloy and an inner rod of copper. In this system, the shock wave propagated through the outer cylinder travels faster than the shock wave propagated through the inner rod, there is conical convergence toward the center, and a high pressure domain called a Mach disk is generated around the central axis.

In this research, we have surveyed traces of Mach disk generation by doing shock recovery experiments with the mousetrap method against the two-layered, cylindrical target. We have also investigated shock wave convergence, the mechanism that generates the Mach disk, by doing mathematical simulations.

2. Methods Used and Content

(1) Shock recovery experiment

The shock recovery experiment was done with the mousetrap flat shock wave generator and momentum trap sample recovery system illustrated in Figure 1. The recovery sample has a two-layered, cylindrical structure with 2024 aluminum alloy as the outer cylinder an internal rod consisting of

either 1) high-grade iron or 2) a SUS304 capsule filled with a mixture of powdered copper and graphite. The speed of the shock wave was measured at 2.1 km/s by the pin contact method.

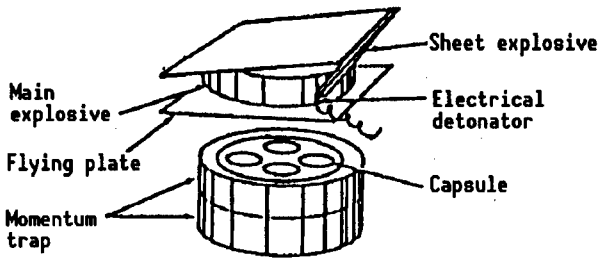

Figure 1. Mousetrap Flat Shock Wave Generator and Momentum Trap Sample Recovery System

(2) Mathematical simulation

Mathematical simulation of the shock recovery experiment was done in order to investigate the mechanism for Mach disk generation. The calculation code used was the two-dimensional shock analysis code, PISCES 2DELK.

3. Results and Observations

(1) Results

As a result of the shock recovery experiment, traces of high-pressure shock compression were found in the high-grade iron and the mixture of powdered copper and graphite. Figure 2 [not reproduced] shows a cross section of a sample with an inner rod of high-grade iron and an outer cylinder of 2024 aluminum alloy. A streamlined region was found that is regarded as showing phase transition, due to the high pressure along the central axis. This result matches, qualitatively, the mathematical simulation. It was also possible to understand the circumstances of Mach disk generation by means of the mathematical simulation.

(2) Observations

The method of generating high pressure by shock wave convergence can be applied to measurement of dynamic properties using shock gun experimental equipment. Moreover, the pressure generated can be further enhanced by the combination of inner rod and outer cylinder materials in a two-layered, cylindrical structure. The selection of materials and the optimum design for the two-layered, cylindrical structure are topics for further study.

Research on Surface Robot Technology (Perception of Environment Using Nontactile Sensors)

93FE0340E Tokyo TECHNICAL RESEARCH AND DEVELOPMENT INSTITUTE, DEFENSE AGENCY in Japanese Nov 92 p 5

[Article by Takao Okui, staff member, Mamoru Furuta, researcher, and Yoshihiro Naito, staff member, 4th Machinery Office, Department 1, Fourth Research Center]

[Text] **1. Objective**

To obtain technical data on environmental perception of terrain forms and obstacles, as element technology for realization of a newly proposed staged structure system for robots that move independently over uneven terrain.

2. Methods Used and Content

(1) Research to achieve the above objective was done by fitting a model robot with a CCD camera and laser range finder as non-contact sensors for perception of the environment.

(2) In this research, the robot's understanding of the environment was divided into the following four stages. In the first stage, uneven terrain is detected. In the second stage, uneven terrain is learned. In the third stage, the distinction is made between even terrain, passable uneven terrain, and obstacles (including impassible uneven terrain). In the fourth stage, the shape of the uneven terrain is understood.

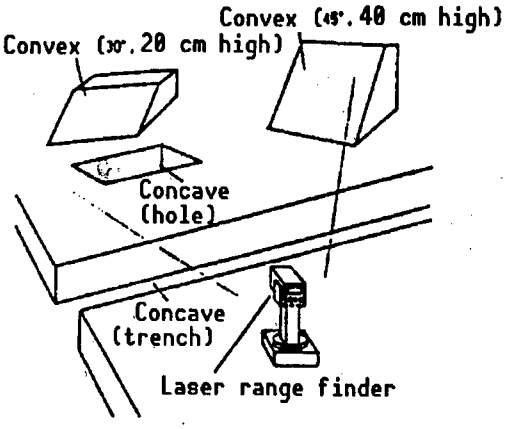

Figure 1. Experimental Model of Uneven Terrain

A basic model of uneven terrain was made in the laboratory using wooden blocks as shown in Figure 1. Experimentation was done, in the first stage, to create a detection algorithm for the color image data obtained from the CCD camera, and in the second stage, to create a learning algorithm from range image data obtained from the range finder.

3. Results and Observations

(1) Results

It was possible to detect uneven terrain by extracting color, physical boundary, and changes thereof from the image data obtained from the CCD camera. By means of preprocessing (including interpolation) and division processing of the distance image information obtained from the laser range finder, it was possible to learn the uneven terrain as shown in Figures 2 [not reproduced] and 3. Those are the basic experimental results obtained.

ID No.	Classi-fica-tion	θ left (deg)	θ right (deg)	Rnear (cm)	Rfar (cm)	H(max) (mm)	D(max) (mm)
1	CONCAVE	-30	30	48	105	-	215
2	CONVEX	-23	-7	169	199	191	-
3	CONCAVE	-22	-1	118	151	-	79
4	CONVEX	13	30	131	199	400	-

Figure 3. Results of Extraction of Landform Information

(2) Observations

Further research in learning uneven terrain will be carried out using a laser range finder and an algorithm will be established. Moreover, by fusing the color image data and distance image data and combining the results with those from contact sensors, a higher level of terrain discrimination will be achieved, and third and fourth stage environmental perception technology will be established.

Research on Centrifugal Explosive Testing (Simulation of Formation of Craters in Sand by Surface Explosions)

93FE0340F Tokyo TECHNICAL RESEARCH AND DEVELOPMENT INSTITUTE, DEFENSE AGENCY in Japanese Nov 92 p 6

[Article by Hiroshi Yamaguchi, Kazuo Fujimoto, Takashi Ito, Masahiro Morishita and Captain Tomonari Nagaai, staff members, Fortifications Research Office, Bureau 1, Fourth Research Center]

[Text] **1. Objective**

Tests with live explosives to evaluate the resistance to explosions of underground defensive structures require large-scale engineering work, and a great investment of manpower and money. For that reason, attention has been paid to reduced scale explosion tests in the laboratory using small amounts of explosive in a centrifugal force field, which allow modeling of explosion tests of large amounts of explosive in real structures. This report deals with (1) confirmation of the utility of centrifugal explosion testing of crater formation by surface explosions, which is an important index for evaluation of the resistance to explosions of underground defensive structures and (2) a method of mathematical simulation to supplement the tests and gain understanding of the detailed behavior of real explosions.

2. Methods Used and Content

(1) Centrifugal explosion testing

The experiments were carried out in a test bunker packed with standard sand using a small centrifugal equipment capable of a maximum 50 G centrifugal acceleration. The explosive was tetryl in four different quantities (0.12 g, 0.61 g, 1.46 g and 4.20 g including the detonator). The explosive was placed in the surface of the sand, and exploded when the desired centrifugal acceleration was achieved. Five levels of acceleration were used: 1 G, 10 G, 25 G, 35 G, and 50 G (in centrifugal explosion tests, when the reduction of scale is 1/N, the centrifugal acceleration is to be NG). The depth, diameter and volume of the crater formed were measured after each explosion.

(2) Mathematical simulation

The general-purpose code for collision phenomena (JDYNA3D) was used for mathematical simulation of a full-scale explosion corresponding to 0.61 g of explosive at a centrifugal acceleration of 50 G. The calculations modeled the formula for the state of standard sand and damage conditions based on past experimental data.

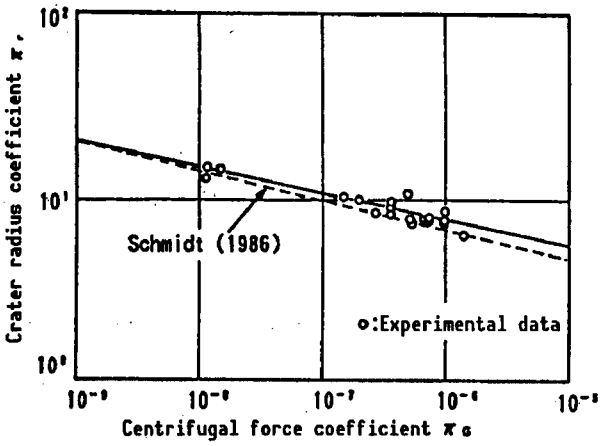

Figure 1. Relationship Between π_G and π_r

3. Results and Observations

Figure 1 illustrates the relationship between the centrifugal force field coefficient π_G (the pi number for gravitational acceleration and the energy of the explosive) and the crater radius coefficient π_r (the pi number for the radius of the crater). The tests confirmed that formula (1), which is shown by the solid line in the Figure, is analogous.

$$\pi_r \cdot \pi_G^{0.141} = 1.120 \quad \text{(correlation coefficient = 0.910)} \qquad (1)$$

Figure 2 illustrates a comparison between the mathematical simulation and test results of crater formation. Because it is difficult to express the dispersion of sand by an explosion in a mathematical simulation, the crater radii were smaller than in the tests, but crater depths were practically the same as in the tests.

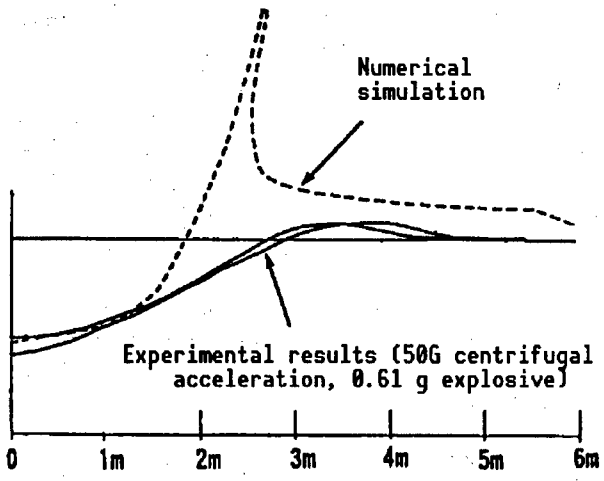

Figure 2. Crater Form

Research on Gas Turbines for Ground Vehicles (Simulation of Nonconstant Performance)

93FE0340G Tokyo TECHNICAL RESEARCH AND DEVELOPMENT INSTITUTE, DEFENSE AGENCY in Japanese Nov 92 p 7

[Article by Yoichiro Shiwa and Soichi Uchida, staff members, 2nd Engine Research Office, Department 2, Fourth Research Center]

[Text] **1. Objective**

Gas turbines have the advantages of small size, light weight, high power and suitability to a variety of fuels; they have great promise as the engines for vehicles of the future. To make them practical, however, it is necessary to explicate engine and transmission control matching characteristics suited to the operating conditions for the vehicles. As the first stage of that process, it is important to explicate gas engine control technology for vehicles. First, it is necessary to know the dynamic characteristics (nonconstant performance) of engines, and to properly explicate simulation technology, including dynamic characteristics, for gas turbine engines for vehicles.

The objective of the present research is to contribute to the optimized design for gas turbine engines for future vehicles through explication of that simulation technology.

2. Methods Used and Content

In this research, a model for hypothesis of nonconstant performance of a gas turbine engine for vehicles was created on the basis of a gas turbine engine of the biaxial free turbine type, with a general purpose heat exchanger. Experimental data from a gas turbine pilot vehicles built for research purposes from FY88 to FY89 was used to verify the suitability of that model. In this model, the characteristics of the components making up the pilot vehicles were shown as mathematical models, and matching was attempted.

3. Results and Observations

(1) Results

There was a good match between the results calculated by the simulation model and the data from acceleration experiments with the pilot vehicles.

(2) Observations

This model can be applied, approximately, as a means for estimating acceleration characteristics of the pilot vehicles. This model will also provide useful data for the optimized design of gas turbine engines for future vehicles.

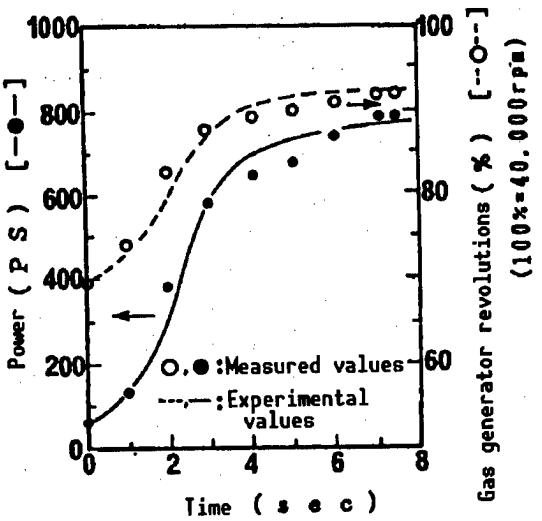

Figure. Acceleration of Pilot Vehicle

We plan to apply operating test data from tracked versions of the pilot vehicle to this model, and to improve the precision of the model by changing the technology level in regard to such things as the thermal resistance limits of the model.

XF3-400 Reheating Turbo Engine

93FE0340H Tokyo TECHNICAL RESEARCH AND DEVELOPMENT INSTITUTE, DEFENSE AGENCY in Japanese Nov 92 p 8

[Article by: Iwao Kashiwagawa, Shunichi Sakuma, Major Mitake Igarashi, Masakore Kitamura and Hidekatsu Kikuchi, staff members, 1st Engine Research Office, Bureau 2, Third Research Center]

[Text] **1. Objective**

A research version of the XF3-400 reheat turbofan engine was fabricated to obtain basic research information on engines for fighter aircraft. The engine was delivered at the end of FY91, and is now being tested within TRDI. This report provides an overview of the XF3-400 engine that has been fabricated.

2. Methods Used and Content

The basic guideline devised for fabrication of the engine was to start with the development technology for the F3 engine for the T-4 intermediate trainer, to add the results of subsequent element research, and to consider these points: a) increasing the overall specific pressure and combustor temperature, b) mounting control equipment and accessories that use digital electronic controls (FADEC) for engine control, and c) reducing engine weight.

The outside diameter of the engine is about the same as that of the F3-30, and new (advanced) technology was incorporated as constituent element technology.

3. Results and Observations

(1) Results

Major engine specifications are shown in the following table. The marked numbers (*) are design values. This engine is the first to be produced in Japan with reheat (afterburner) equipment and digital electronic control equipment with hydraulic backup.

Table. Major Specifications

Item		Specification
Length, with nozzle (mm)		2,927
Maximum diameter (mm)		660
Thrust (kgf)	Without reheat With reheat	2,180* 3,490*
Thrust-weight ratio		7.0

(2) Observations

New technology was adopted in this engine. In addition to scrutinizing functions and performance in internal testing, it was possible to confirm the technology for integration of elements. The results will be reflected in R&D on even more advanced engines in the future.

Research on Ramjet Engine Combustors

93FE0340I Tokyo TECHNICAL RESEARCH AND DEVELOPMENT INSTITUTE, DEFENSE AGENCY in Japanese Nov 92 p 9

[Article by Yokichi Sugiyama, Hiroaki Hasegawa and Katsumi Adachi, staff members, 4th Engine Research Office, Bureau 2, Third Research Center]

[Text] **1. Objective**

The operating conditions required for combustors for ramjet engines, which show promise as engines for guided missiles of the future, include reliable ignition, stable combustion and high combustion efficiency. In the research reported here, combustion tests were conducted on a ramjet engine combustor of the type with four lateral air intakes.

2. Methods Used and Content

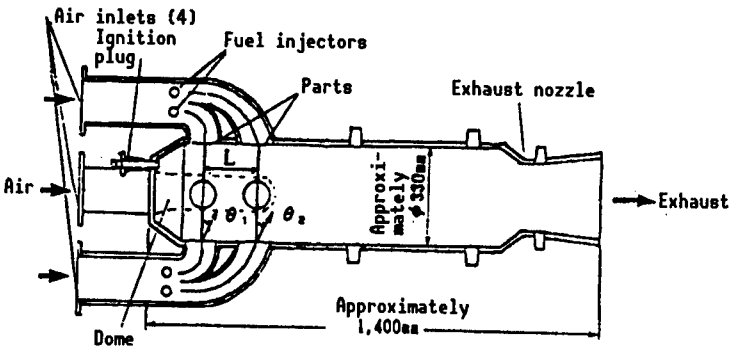

Figure 1. Test Combustor

In consideration of integration (incorporation of boosters) the combustor in question (Figure 1) is cylindrical, and the air from each of the four intakes is divided into two streams (one forward of the other), for a total of eight ports into the combustor; fuel jets are located where the streams divide. The design is such that a part of the air mixture entering through a forward port circulates back to form an eddy in the forward end (dome) of the combustor, where it is ignited. The air (or air mixture) from the rearward port is used to complete combustion.

In this research, the airflow conditions modeled flight at about Mach 2 at an altitude of 30,000 feet. Combustion tests were conducted with various combinations of port separation L, intake angle θ and different port areas, the fuel-air ratio being varied from the thinnest that would sustain ignition up to the theoretical maximum.

3. Results and Observations

(1) Results

In all cases, good ignition could be confirmed down to extremely low fuel-air ratios, and a fairly high fuel efficiency (Figure 2) could be obtained within the range of fuel-air ratios that would actually be used (from about 0.03~0.07). It was learned, however, that when the port separation L or intake angle θ were great, there was a tendency to oscillating combustion at higher fuel-air ratios.

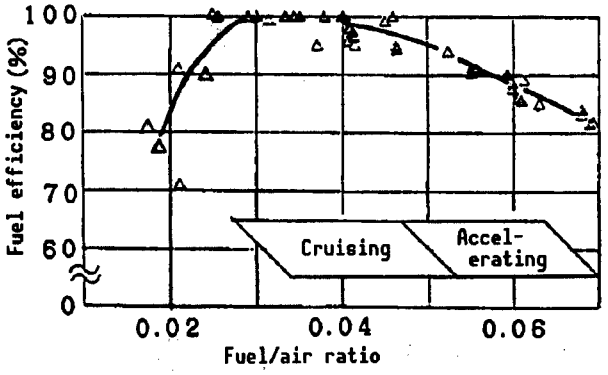

Figure 2. Example of Test Results

(2) Observations

Valuable technical data was obtained that will assist further research on ramjet engine combustors having four lateral air intakes.

Design of Robust Autopilot With Self-Learning Application Mechanism

93FE0340J Tokyo TECHNICAL RESEARCH AND DEVELOPMENT INSTITUTE, DEFENSE AGENCY in Japanese Nov 92 p 10

[Article by Toshiyuki Tanaka and Yasutaka Aizawa, staff members, 1st Guidance Research Office, Department 3, Third Research Center]

[Text] **1. Objective**

In order to reduce the miss distance of missiles with a broad interception range, it is necessary that sensitivity not be dulled when there are great changes in the missile's flight environment (dynamic pressure and Mach number). Moreover, stable flight requires that the response to changes in the flight environment not be too rapid. This autopilot maintains responsiveness at a fixed level by means of an adaptability structure based on the dynamic pressure and Mach number hypothesized from speed and altitude information. A notable feature is the use of autopilot control logic combined with the "neurofuzzy" method to provide adaptability through self-learning.

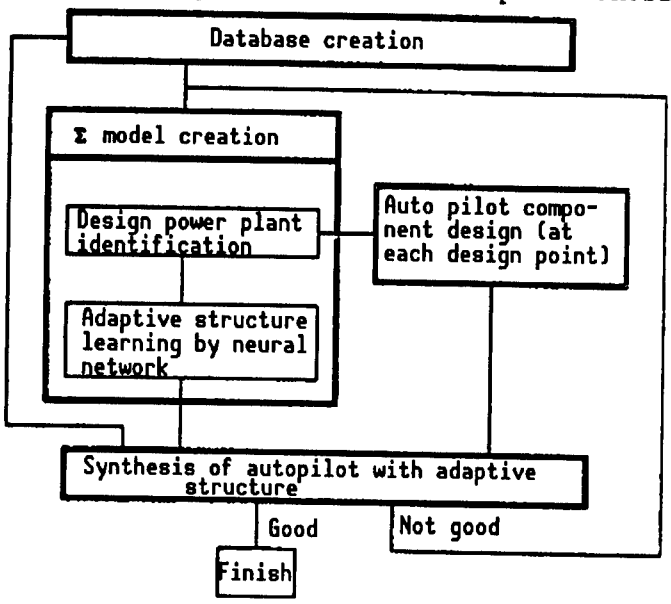

Figure 1. Diagram of Four Steps of Design Method

2. Methods Used and Content

This design method consists of four steps (Figure 1): 1) For database generation, it is necessary to accumulate data from wind tunnel tests and firing (flight) tests using the following steps; 2) For Σ-model generation, learning is done with a neural network that simulates system identity and adaptability structure under the design conditions selected. 3) In the design of autopilot components, the autopilot is designed using a robust

control logic appropriate to the design conditions. 4) An autopilot having the applicability structure is generated by synthesizing the results of 2) and 3), and evaluated using the database obtained in 1). Figure 2 shows a closed loop block diagram. The various components are weighted by means of functions f_1 through f_n.

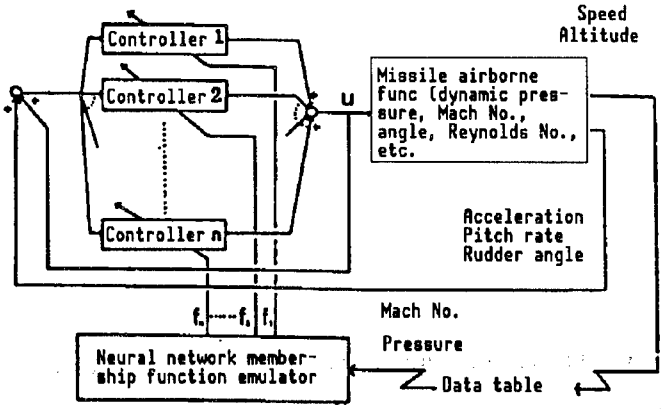

Figure 2. Closed-Loop Block Diagram

3. Results and Observations

(1) Results

H-infinity control theory was used in the design of each design point. Figure 3 is an example of simulation of rotational acceleration of the flying body in response to rotational acceleration commands at 0.6 Mach with dynamic pressure between 100~700 psf when there is uncertain information on aerodynamic pressure and altitude.

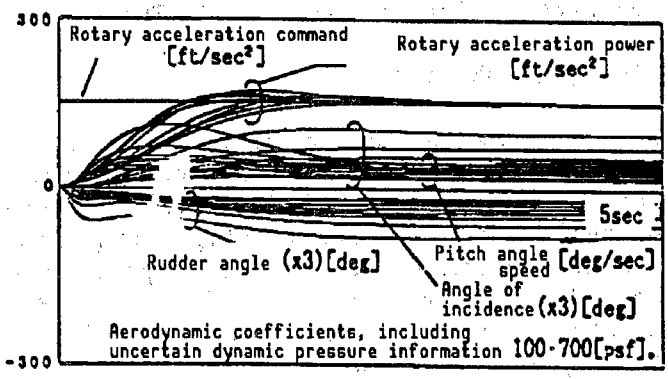

Figure 3. Results of Simulation

(2) Observations

The results of the simulation confirmed that an autopilot had been designed with a robust and low-sensitivity adaptability structure and practically uniform response to acceleration commands in the face of changing altitude and speed, and even in the event of uncertainty regarding dynamic pressure and altitude information.

Basic Research on Active Laser Seeker With Three-Dimensional Image

93FE0340K Tokyo TECHNICAL RESEARCH AND DEVELOPMENT INSTITUTE, DEFENSE AGENCY in Japanese Nov 92 p 11

[Article by Hiromoto Hokazono and Moriyoshi Yamakawa, staff members, 3rd Guidance Research Office, Department 3, Third Research Center]

[Text] **1. Objective**

With the emergence of semiconductor laser (LD) pumped solid lasers in recent years, it has become possible to obtain highly efficient, high-powered laser beams from extremely compact laser equipment. Active laser seekers, which had previously been considered impractical in terms of size and efficiency, have thereby finally become practical. LD pumped solid lasers that have experienced rapid improvement in performance with the progress of research in recent years include Nd:YAG(1.06μ), Nd:YVO_4(1.06μ), Er:Glass(1.55μ), Er:YAG(1.66μ), Tm:YAG(2.02μ) and HO:YAG(2.13μ). As seen in Figure 1, these lasers emit in near-infrared wavelengths with good atmospheric transmittance; all these lasers are applicable to homing seekers. The greatest advantage of active laser seekers is that scanning with the transmitted laser beam simultaneously provides both image information on the distance to the target and background and two-dimensional image information corresponding to the received intensity of the laser beam. Thus, three-dimensional imagery that includes range to the target and background can be obtained easily from a single laser emitter and receiver set. Use of three-dimensional image information is expected to markedly improve capabilities, such as locking on ground targets or evading obstacles, that were very difficult to achieve using only two-dimensional images from infrared or visible light in earlier passive seekers. The objective of the

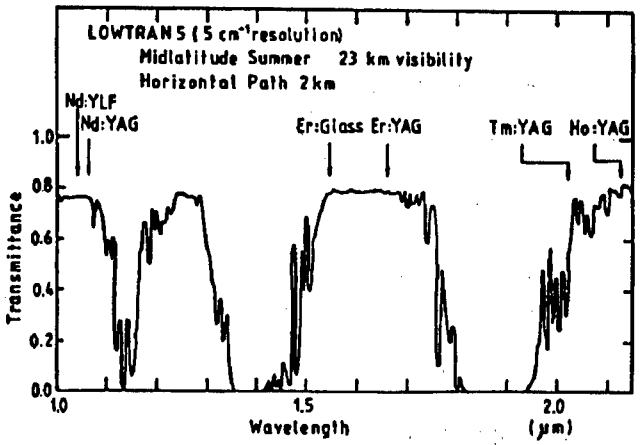

Figure 1. Emission Wavelength and Atmospheric Transmittance of LD Pumped Solid Lasers

present research is a theoretical explanation of the relationship between laser power and detectable distance, as a first step in research on active laser seekers that have these advantages.

2. Methods Used and Content

A detailed mathematical model based on laser radar formulas was created to explain the relationship between laser power and detectable distance. The lasers used were Nd:YAG and Nd:YVO_4 (both 1.06μ). The detector was assumed to use an Si avalanche photodiode (APD) capable of achieving a high S/N ratio at that wavelength. The detection method was direct detection, considering the placement in relatively small missiles, rather than heterodyne detection with a complex optical system. An improved LOTRAN5 model with resolution of 5 cm^{-1} was used for correction of atmospheric transmittance.

3. Results and Observations

Figure 2 shows the results of calculation of S/N ratio in relation to incident laser power when Si ADP noise (Schottky noise from background light, target reflected (signal) beams and dark currents, and preamplifier Johnson noise) was taken into consideration. As is clear from Figure 2, the S/N ratio is reduced markedly by background light. It was learned that because of the great background light power in the near-infrared region of sunlight, it would be necessary to use an optical filter during daylight to exclude background light. This report deals with the relationship between laser power and detectable distance with the use of a suitable optical filter.

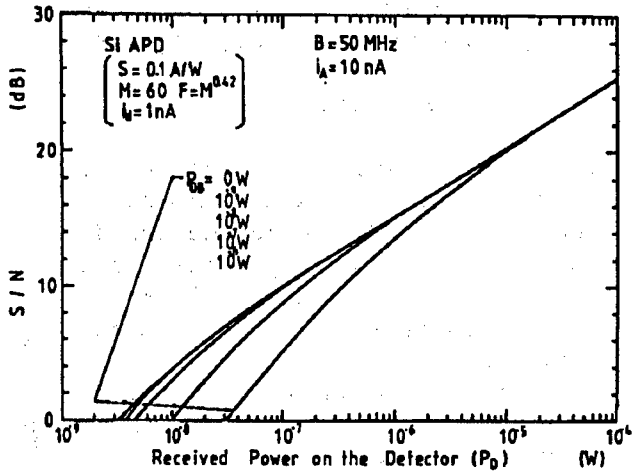

Figure 2. Relationship of Received Laser Power and S/N (P_{DB} is background power at the detector face.)

Research on Constituent Elements or Ku Band Seeker

93FE0340L Tokyo TECHNICAL RESEARCH AND DEVELOPMENT INSTITUTE, DEFENSE AGENCY in Japanese Nov 92 p 12

[Article by Kazuo Komata and Hidehiko Kubo, staff members, 4th Guidance Research Office, and Keizo Suzuki, departmental chief researcher, Department 3, Third Research Center]

[Text] **1. Objective**

Superior detection capability is necessary for an electromagnetic seeker to deal with a small, high-speed target. Means considered to achieve that include increased transmission power and improved direction gain, but current X band seekers have been pushed close to their limits. A shift to the Ku band can be expected to improve performance within current fuselage diameters because of the increased mounting density of modules and the multiplication of transmission power and directional gain. We therefore fabricated and tested antennas, phase shifters and other constituent elements necessary to realization of a Doppler tracking-type Ku band seeker with an electronic scanning antenna, and can report that good results were obtained. The antenna, incidentally, was studied on the premise that both the Ku band in the active mode and the X band in the passive mode would be covered.

2. Methods Used and Content

The antenna mode adopted was a compact, dual-use patch antenna. Consideration was given to an antenna structure for which both an improved utilization factor (Ku band and X band through a single aperture) and minimal effect on the pattern from mutual interference could be expected. Antenna configurations were fabricated in two promising proposals: a structure in which Ku and X band antenna elements were arrayed in a single plane, and a structure in which the X band antenna array was stacked on top of the Ku band antenna. Then the patterns of each were measured. A distributed comparator planar circuit for monopulse processing of Ku band and X band constituents was fabricated, as were a hybrid phase shifter for electronic scanning in the Ku band, and a compact transmission source for active use, and various basic characteristics of each were measured.

3. Results and Observations

(1) Figure 1 is a structural diagram of an antenna constructed with both Ku and X band antenna elements arrayed in a single plane. Figure 2 shows the results of measurement of the pattern of that antenna. The structure in which the arrays of Ku band and X band antenna elements were stacked showed similar characteristics.

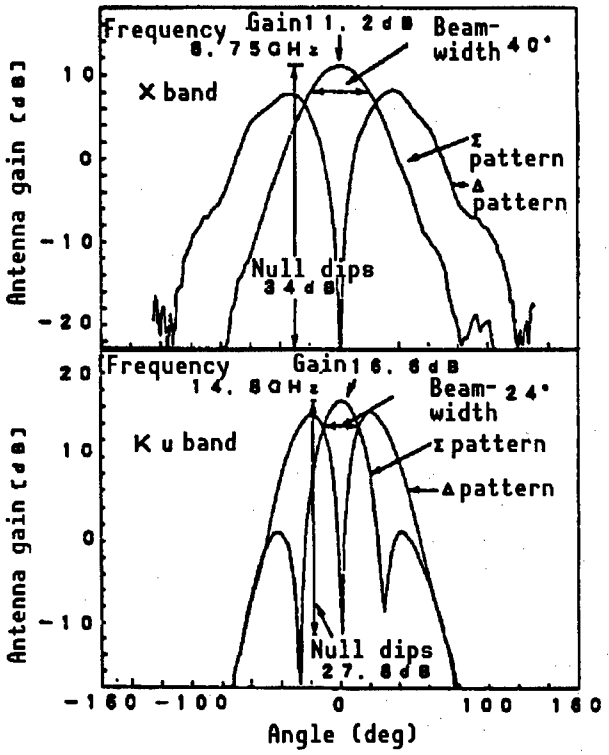

Figure 2. Planar Array Antenna Pattern Characteristics

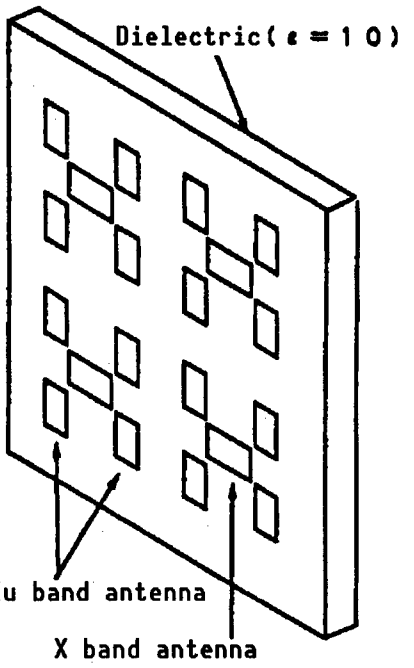

Figure 1. Antenna Structure in Planar Array

(2) It was confirmed that the Ku band hybrid phase shifter had superior linearity with very small quantization errors.

(3) Excellent characteristics were confirmed for the transmission source and distributed comparator for two-frequency monopulse processing.

The results described above offer prospects for realization of the basic elements, including the transmission and reception system, of a phased-array, strapdown-type Ku and X band dual frequency seeker. Future efforts are expected to reduce the size and increase the power of the Ku and X band dual frequency module, including the transmission and reception system, in consideration of use on smaller missiles. Other goals are incorporation of signal processing technology of the frequency dispersion type, and improved detection capability and ECCM properties in a small size.

Automatic Discrimination of Modulation Method for Digital Communications

93FE0340M Tokyo TECHNICAL RESEARCH AND DEVELOPMENT INSTITUTE, DEFENSE AGENCY in Japanese Nov 92 p 13

[Article by Hitoki Takeda, Yasufumi Onishi and Masaki Ishikawa, staff members, 2nd Information Research Office, Department 1, Second Research Center]

[Text] **1. Objective**

There is a worldwide trend toward digitization of communications to cope with the great increase in the volume of communications, the diversification of information media and improvement of signal quality. Various modulation methods have been adopted for digital communication, with modulation of amplitude, frequency and phase. When radio waves are monitored, however, digital communications differ from analog communications in that multiplexing is not possible unless the modulation method and parameters are all the same, and so it is generally necessary to have different communications equipment for each method of modulation.

The research reported here was to devise a method to infer the method of modulation of digital communications encounter when monitoring radio signals, and to automatically discriminate among a variety of modulation methods.

2. Methods Used and Content

The automatic discrimination method adopted in this research applied an expert system. The test system, which used simulation, is shown in Figure 1. It was thought that if actual communications signals were used in tests, peripheral noise would be added in, and so the characteristics of modulation methods shown in the I–Q pattern (see Figure 2) would be obscured. In the test system, therefore, attention was paid to ways to enhance the precision of judgements in the inference section.

3. Results and Observations

(1) Results

Automatic discrimination was analyzed in circumstances where the simulated communications signal consisted of FSK or PSK modulated digital signals

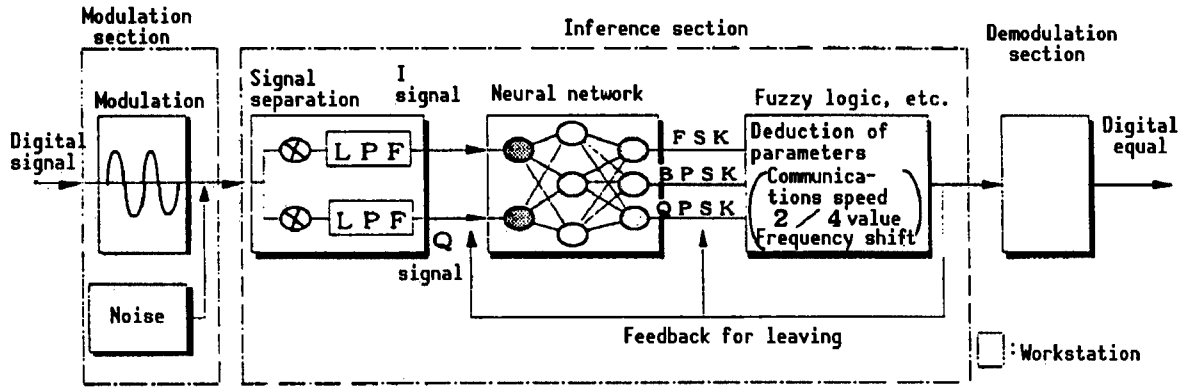

Figure 1. Test System

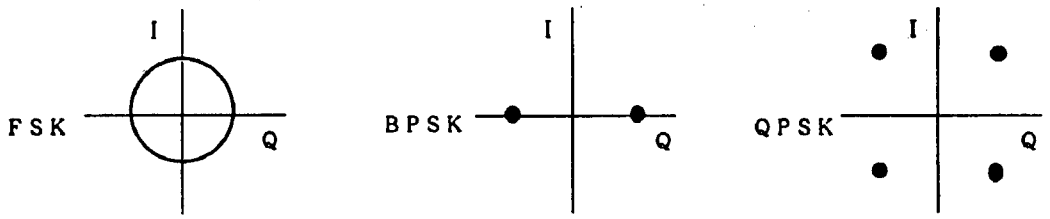

Figure 2. I-Q Pattern (Sample)

overlaid with white noise, and the S/N ratio was varied. The result was that practically perfect discrimination was possible when S/N = ∞ (no noise), and there were prospects for discrimination at a practical level even when the S/N ratio was between 40 and 30 dB.

(2) Observations

Experimentation will continue using actual digital communication signals, and so it expected that discrimination capabilities will be improved to handle higher noise levels.

Radar Signal Processing Using Linear Prediction Method

93FE0340N Tokyo TECHNICAL RESEARCH AND DEVELOPMENT INSTITUTE, DEFENSE AGENCY in Japanese Nov 92 p 14

[Article by Hideaki Watanabe, Fujiro Shimano, Major Kunio Asami and Kiyomasa Abe, staff members, 2nd Radio Research Office, Department 2, Second Research Center]

[Text] **1. Objective**

High-resolution frequency estimation methods using linear prediction have been established in research areas like signals theory in recent years. Application of this method has begun to become practical in regard to speech processing, ground wave analysis, radar signal processing and so on. This report announces research in application of this method to radar clutter suppression and array antenna beam formation.

2. Methods Used and Content

(1) Application to radar clutter suppression

In the past, clutter suppression has performed signal processing using MTI (moving target identification) and FFT (fast Fourier transform), but there is a problem with that method in that it cannot handle moving clutter such as rain clouds. That is because MTI signal processing sets up filters for fixed clutter and can suppress clutter where the doppler shift of reflected radar signals is close to 0 Hz (fixed clutter), but is unable to suppress other (moving) clutter. With the linear prediction method, clutter suppression filter characteristics can be varied by minimizing clutter output power; an adaptive MTI capable of suppression processing of moving clutter can be achieved.

(2) Application to beam formation

By applying the high-resolution frequency estimation method to array antennas, it is possible to estimate with high resolution the direction from which a radio signal comes. This is a major improvement from the past, when the resolution of directionality was limited by the size of the antenna.

3. Results and Observations

(1) Application to clutter suppression

The effectiveness of adaptive MTI using the linear prediction method was confirmed on the basis of real clutter data obtained with clutter suppression test equipment. Consequently, it was confirmed that good clutter suppression results can be obtained against various types of clutter (ground clutter, sea clutter, weather clutter).

(2) Application to beam formation

Regarding high-resolution processing, it was confirmed using simulations that processing can be done with much higher resolution than with conventional means.

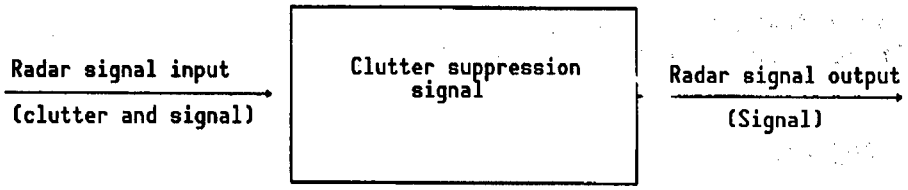

Figure. Minimization of Clutter

Formation of Aerial Beam Applying Fuzzy Design Method

93FE03400 Tokyo TECHNICAL RESEARCH AND DEVELOPMENT INSTITUTE, DEFENSE AGENCY in Japanese Nov 92 p 15

[Article by Tamotsu Araki, staff member, 3rd Radio Research Office, and Takashi Mayama, Masaaki Sugano and Shigeru Suzuki, staff members, 4th Radio Research Office, Department 2, Second Research Center]

[Text] **1. Objective**

In conformal array antennas suited to the external shape of aircraft or ships, side lobe reduction and null point formation are important issues from the perspective of elimination of unnecessary radiation. This paper reports the results of studies of a method of beam pattern correction that uses fuzzy design and an algorithm for amplitude and phase control that can achieve formation of the desired beam in respect to surfaces with multiple curves.

2. Methods Used and Content

The directionality algorithms for many conformal arrays project elements from the desired curve to the aperture plane, correct the element density and element patterns, then hypothesize a better solution on the basis of planar projection to find the amplitude distribution to give reduced side lobes. There is, however, no guarantee that this is the conformal array's optimal pattern. Consequently, improvement was made to the algorithm for output power minimization with lock conditions by using fuzzy numbers for lock conditions and adding fuzzy rules for new side lobe levels. Then, taking this issue as a fuzzy design method, sensitivity analysis is performed to elicit an algorithm to learn the amplitude and phase

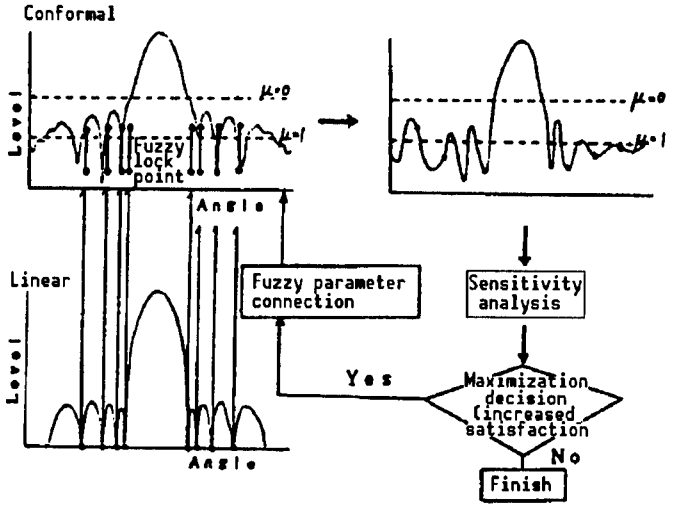

Figure. Concept of Beam Formation Algorithm

distribution of array elements to obtain the desired pattern, in the sense of improving the degree of satisfaction of these rules (see Figure).

3. Results and Observations

It was confirmed that limiting the fuzzy numbers in the direction that increased the degree of satisfaction of all rules could simultaneously meet conflicting demands, such as reduced side lobes and high gain. The formation of null points for unwanted radiation is to be included in the rules hereafter.

Research on Millimeter Wave Band Propagation Characteristics

93FE0340P Tokyo TECHNICAL RESEARCH AND DEVELOPMENT INSTITUTE, DEFENSE AGENCY in Japanese Nov 92 p 16

[Article by Nobukore Oshima, Minoru Toshida and Shojiro Inoue, staff members, Electromagnetic Properties Research Office, Iioka Branch, Second Research Center]

[Text] **1. Objective**

Radio propagation in the millimeter wave band enables the easy transfer of large volumes of information with small, light-weight equipment, and as radar it provides high resolution. But because propagation losses vary greatly with weather conditions like rainfall, it is necessary to have a full understanding of propagation characteristics when using millimeter waves. This report concerns the measurement and analysis of millimeter wave propagation losses during rainfall.

2. Methods Used and Content

The "millimeter wave band characteristics evaluation equipment (part 1)" was fabricated to simultaneously measure weather conditions and the propagation losses of millimeter waves (36 GHz, 60 GHz and 94 GHz bands). A block diagram of this equipment is shown in Figure 1. The transmitter portion was mounted on a steel tower at the Iioka Receiving Station, and the receiver portion was set up on the fifth level of an experimental tower at the Iioka branch of the Second Research Center (with a separation of 2,841 m). Propagation losses from horizontal and vertical polarization were measured for each of the three frequency bands. Intensity of rainfall was measured at the transmitter end, and the meteorological portion at the receiver end recorded such measurements as rainfall intensity, air temperature, humidity, wind direction, wind speed and air pressure.

3. Results and Observations

(1) Results

From analysis of the results, it was confirmed experimentally that there are correlations between rainfall intensity and rainfall-based attenuation, and

between frequency and rainfall-based attenuation. A sample of the measurements (rainfall intensity and rainfall-based attenuation) is shown in Figure 2.

(2) Observations

Rainfall-based attenuation α is in the relationship $\alpha = aR_b$ (where R is the rainfall intensity and a and b are functions for frequency and temperature), with a and b found by fitting measured data to the formula by the least squares method. These values a and b differ depending on the day of measurement. The diameter of the raindrops is thought to be one factor in this. Further analysis will be done to take raindrop diameters into account.

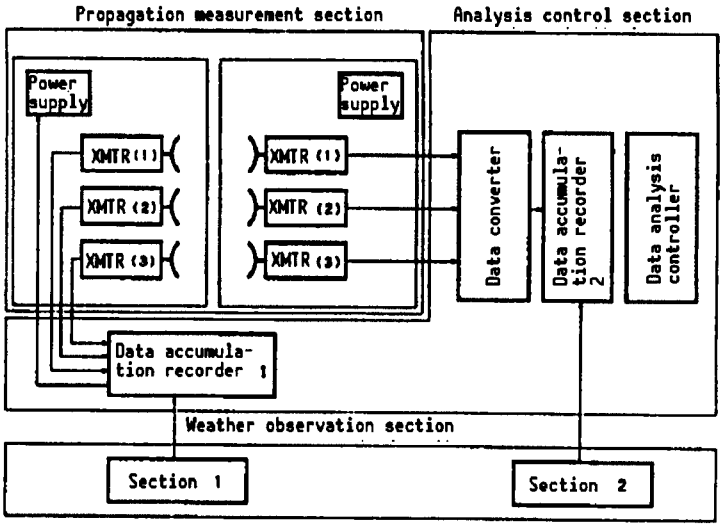

Figure 1. Block Diagram of Millimeter Wave Band Characteristics Evaluation Equipment (Part 1)

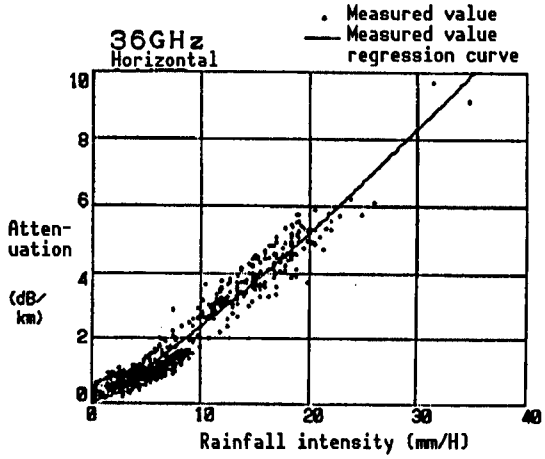

Figure 2. Rainfall Intensity and Rainfall-Based Attenuation

Inquiry on Aerodynamic Measurement of Ram Air Parachutes

93FE0340Q Tokyo TECHNICAL RESEARCH AND DEVELOPMENT INSTITUTE, DEFENSE AGENCY in Japanese Nov 92 p 17

[Article by Hidetake Kuwano and Chikashi Saito, staff members, Parachute Research Office, Department 3, First Research Center]

[Text] **1. Objective**

With conventional parachutes, the primary design elements are deployment characteristics, stability and landing characteristics. In the case of ram air parachutes, however, gliding and steering characteristics must be taken into consideration as well. This report, therefore, considers the aerodynamic design of gliding and steering characteristics of ram air parachutes following deployment.

2. Methods Used and Content

The simplified airframe model shown in Figure 1 was established for consideration of the aerodynamics of ram air parachutes. This airframe model comprises a two-dimensional, wing-shaped canopy, a representative suspension line and a suspended payload. The representative suspension line connects a point one-fourth the chord of the canopy with the center of gravity of the suspended payload. The angle of the airframe axis through the representative suspension line and the one-fourth chord length point to a vertical axis (the rigging angle) is ϕ.

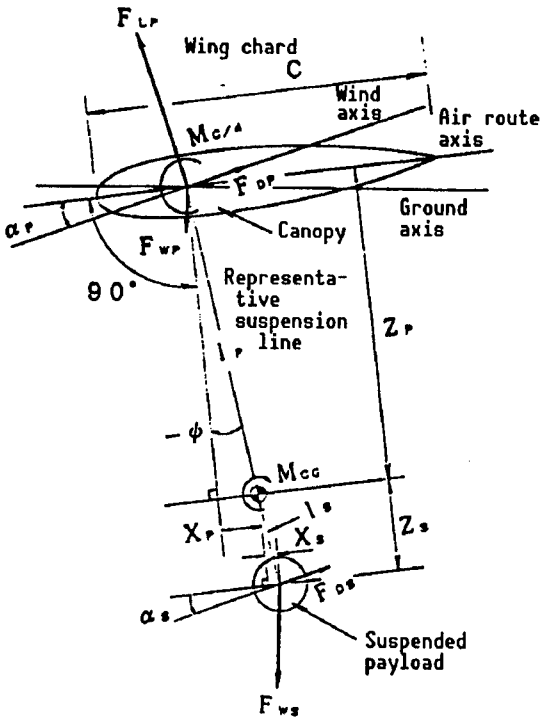

Figure 1. Simplified Airframe Model

The aerodynamic study of ram air parachutes was carried out using ram air parachute low-speed wind tunnel experimental data from FY90 and a simple airframe movement simulation program for ram air parachutes developed in FY91.

3. Results and Observations

(1) Results

a) It was learned that the rigging angle plays a great role in the gliding characteristics of ram air parachutes.

b) Changes in the pull on the left and right steering lines did not produce abnormal movement in airframe flight in the simple airframe movement simulation program for ram air parachutes, and it was learned that the ram air parachute is a flying body with relatively good stability.

(2) Observations

a) Wing surface load was not taken into consideration in this aerodynamic design of ram air parachutes; it will be necessary to consider optimum wing surface load hereafter.

b) It will be necessary, when gathering aerodynamic data for reduced scale ram air parachutes, to do further research on test methods (such as wind tunnel experiments) that allow the gathering of data in conditions closer to reality.

High-Speed SES Water Jet Inlet Duct Formation

93FE0340R Tokyo TECHNICAL RESEARCH AND DEVELOPMENT INSTITUTE, DEFENSE AGENCY in Japanese Nov 92 p 18

[Article by Tatsuo Kashiwadani, staff member, 2nd Fluids Research Office, Department 4, First Research Center]

[Text] **1. Objective**

SES propulsion equipment that runs at high speeds often makes use of water jets because of the superior cavitation characteristics. Depending on the shape of the inlet that conducts water to the water jet pump, however, there is liable to be partial cavitation because of a marked pressure drop. It is thus necessary to design this part with great care to minimize cavitation. This task is of particular importance in the design of the high-speed SED intended to speed up the experimental ship *Meguro*.

The author had previously considered means of design shapes with little pressure drop by logical calculation of two-dimensional flows, and had studied high-speed SES inlet shapes. This has yielded shapes that are superior in terms of calculations. In the present research, wind tunnel tests have been performed on inlets having shapes obtained in this way, and study has been given to anti-cavitation properties in actual flows influenced by three-dimensional effects and viscosity; the results are reported here.

2. Methods Used and Content

In studying of the generation of cavitation, it is preferable to experiment using a cavitation tank that can actually produce cavitation, but in the initial phase of shape studies, it is effective to study anti-cavitation properties by measuring the pressure distribution of the flow. In this study, therefore, wind tunnel testing was done using a 1/2.5 reduced scale model (Figure 1) of the inlet of the high-speed SES experimental ship. The pressure distribution on the inlet surface was measured

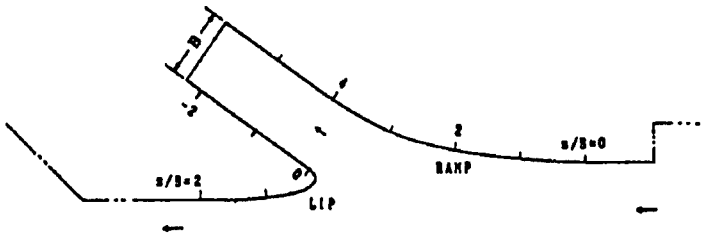

Figure 1. Shape of Inlet Channel

for various intake intensities (IVR), and the potential for generation of cavitation was studied.

3. Results and Observations

(1) Results

Figure 2 shows the measured values of pressure distribution on the inlet surface at the design point of IVR = 0.75.

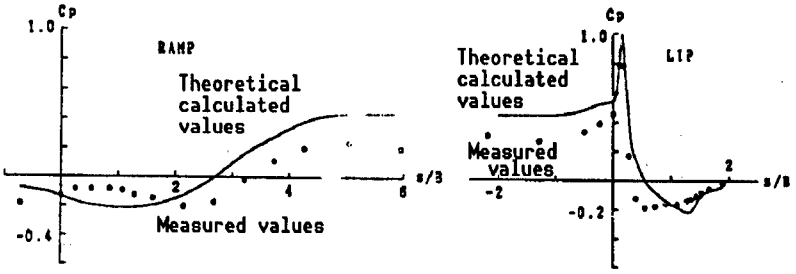

Figure 2. Results of Wind Tunnel Test

(2) Observations

There was some difference of distribution between the measured results and the two-dimensional theoretical calculation; the measured minimum pressure was somewhat higher, and the shape was found to be superior. It was confirmed, as a result, that there is the possibility of running cavitation-free up to 60 knots.

Acoustic Characteristics of Anisotropic Hull Plate Model

93FE0340S Tokyo TECHNICAL RESEARCH AND DEVELOPMENT INSTITUTE, DEFENSE AGENCY in Japanese Nov 92 p 19

[Article by Yoshio Okamoto, Kazuhiko Kuda and Akira Ichiyanagi, staff members, 2nd Structural Research Office, Bureau 4, First Research Center, and Atsuhiro Tsutsumi, technical information specialist, 2nd Technology Division, Technology Bureau]

[Text] **1. Objective**

The reduction of noise emitted into the water by ships is extremely to prevention of detection. The noise emitted into the water by the vibration of equipment on board is the biggest factor within the category of mechanical noise. Knowing the emission characteristics of noise emitted from the hull below the water line is extremely important for reduction of such vibrations. The hull below the water line is normally constructed of plates reinforced by ribs or framing. Until the last fiscal year, our research was done on the acoustic properties of long plates, simulating hulls reinforced only with ribs.

This report deals with anisotropic plates, simulating a hull reinforced with ribs and frames, and experimental study of the effect of rigidity on the acoustic properties when vibration is applied to such plates.

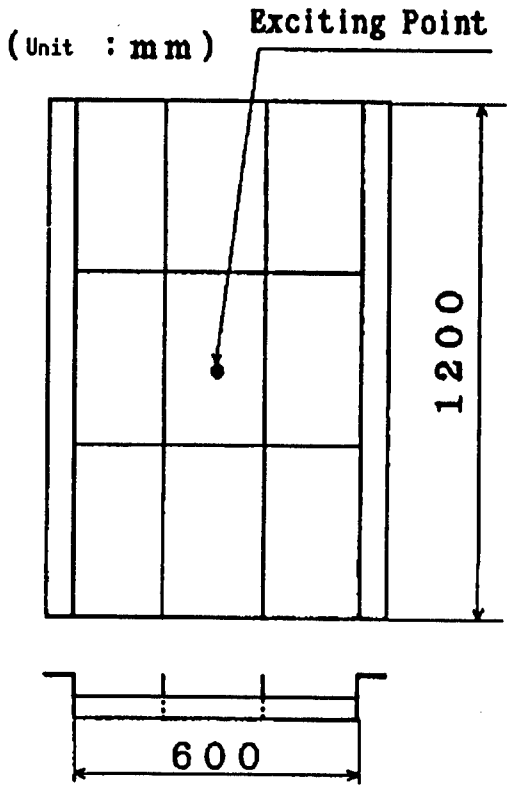

Figure 1. Layout of Test Structure

2. Methods Used and Content

A scale model was created on the basis of the rib and frame spacing and plate thickness of an actual ship, and five other

models were built with different spacings or plate thickness (Figure 1). Vibration was applied to the centers of the models; acoustic intensity was measured in three dimensions, and patterns of acoustic emission were compared. To simulate double hulling, second plates were added, and the same comparisons were made using indirect vibration.

3. Results and Observations

(1) Results

An example of the acoustic emission patterns is shown in Figure 2.

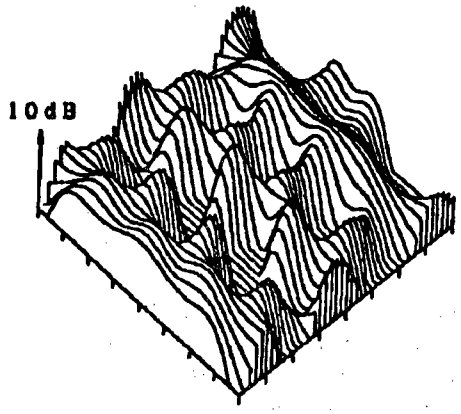

Figure 2. Sample Acoustic Emission Pattern

a) Except to the immediate area of the excitation point, there was practically no difference in acoustic emission properties between direct vibration and indirect vibration.

b) Emission patterns changed with different rib and frame spacing, but similar emission patterns were seen in the high-frequency region.

(2) Observations

It was confirmed that the acoustic intensity method is effective for judging the effect of the rigidity of reinforcing structures on the reduction of noise emitted into the water from the outer plate of hulls.

Eye-Safe Optical Parametric Oscillator

93FE0340T Tokyo TECHNICAL RESEARCH AND DEVELOPMENT INSTITUTE, DEFENSE AGENCY in Japanese Nov 92 p 20

[Article by Kiyoshi Kato, chief researcher, Department 3, Second Research Center]

[Text] **1. Objective**

The recent rapid developments in eye-safe lasers include KTP optical parametric oscillation (OPO) excited by Nd:YAG lasers. High conversion efficiencies of about 70% have been obtained in the regions of 1.6 and 3.2 μm, and they are already in use as the optical source for imaging laser radars. But because the infrared absorption band of KTP crystals is close to 3 μm, the 3.26 μm idler at the 90° phase adjustment point where the conversion efficiency is greatest, laser damage occurs rapidly and it is difficult to obtain stable power over a long period. For that reason, a number of countries have worked to develop infrared, nonlinear optical crystals to replace KTP. The author, using RTP crystals ($RbTiOPO_4$) has solved this major problem, and will report in detail on RTP/OPO (patent applied for).

2. Methods Used and Content

The RTP crystal used in this experiment was grown by the flux method, with x=13, y=z=6 mm, and the yz (bc) face optically polished to a precision of $\lambda/10$ to maximize the effective nonlinear optical constant d_{eff}, and coated with a wideband anti-reflection film with a 1.3 μm central wavelength. Prior to 1.064 μm pump OPO, there was an OPO experiment excited with a low 0.532 μm oscillation threshold; a dispersal formula for the non-linear optical constant and index of refraction was obtained. As a result, it was learned that the nonlinear optical constant of RTP is 10% greater than that of KTP. The properties obtained so far with an x-cut sample at P_p=250 MW/cm^2 are 30% peak conversion efficiency, 0.7 W maximum average power (signal + idler), ±7% power stability, and about 3 Å spectrum width of resonant signal beam. Moreover, the OPO oscillation threshold is practically the same as the best 1.5 cm KTP crystal.

3. Results and Observations

Exciting an x-cut RTP at the 1.064 μm basic wavelength of Nd:YAG lasers, a 10 MW peak power and 0.7 W average power pulsed infrared was obtained at λs=1.627 and λi=3.077. Because the temperature dependence of the oscillating wavelength in this system is 0 and the idler is outside the absorption band characteristic of RTP, extremely stable how power is possible. Consequently, if combined with commercially available LD excited Nd:YAG lasers, oscillation at a high repetition rate of about 10 kHz is possible without cooling, and the 1.63 μm device can be applied to eye-safe lasers or laser designators, and the 3.08 μm device is tunable to 3.6 μm and so can be used as an optical source for laser jammers.

Real-Time Control of Laser Convergence Characteristics With Supplementary Optical Compensation System

93FE0340U Tokyo TECHNICAL RESEARCH AND DEVELOPMENT INSTITUTE, DEFENSE AGENCY in Japanese Nov 92 p 21

[Article by Masakatsu Sugii, Yasuaki Mine, Katsuhiko Komatsu and Hideaki Saito, staff members, 2nd Optical Research Office, Department 3, Second Research Center]

[Text] **1. Objective**

We fabricated a optical compensation system of the multi-dither type for the purpose of correcting shape distortion by the optical convergence system or distortion of laser convergence characteristics that occur during atmospheric propagation. Having conducted tests of control system optimization, static phase distortion and dynamic phase distortions modelled on atmospheric fluctuation, we report that the effectiveness of the system has been confirmed.

2. Methods Used and Content

A block diagram of the optical compensation test equipment fabricated for this research is shown in Figure 1. The compensation system is an active optical control system that performs real-time detection of phase distortion from atmospheric fluctuation or other causes, calculates the amount of phase correction by signal processing equipment, and controls multiply divided optical compensation system mirrors to correct for spatial wave distortions and enhance peak laser intensity at the convergence point. The multi-dither method is a phase detection system that applies minute oscillation (dithering) to the extent of 1/20 the wavelength at a given frequency to the each of the mirrors of the

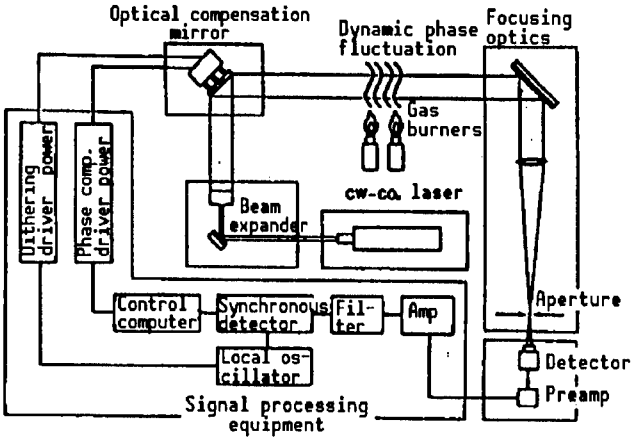

Figure 1. Block Diagram of Experimental Equipment

optical compensation system, and indirectly detects phase distortion from the brightness modulation component generated by the prominence of laser beams from the small apertures at the convergence point. By controlling the optical compensation system so as to minimize the amplitude of the brightness modulation component of each mirror, it is possible to spatially align the phases at the convergence point.

3. Results and Observations

First the control system was optimized and compensation of static distortion generated in the light path was tested using a Ge phase sheet. The result was high compensation, nearly at the theoretical value.

Next, gas burners were used to create dynamic phase distortion, simulating atmospheric fluctuation, in the light path and compensation testing was performed. The compensation time was 55 ms using the saturation properties of the optical detector, which was shortened by a factor of 16 from the unsaturated value of 830 ms. Compensation tests were conducted on dynamic phase distortion using this high-speed compensation control method. Figure 2 shows the convergence pattern at the plane of the convergence point before and after compensation (14 ms sampling time). It is clear from this Figure that the beam convergence pattern following compensation is changed almost to the Airy disk pattern at the limits of refraction. It was also confirmed, by temporal variation of the detector signal intensity before and after compensation and temporal variation of the 1/f fluctuation component included in the frequency spectrum, that compensation of dynamic phase distortion simulating atmospheric fluctuation is possible.

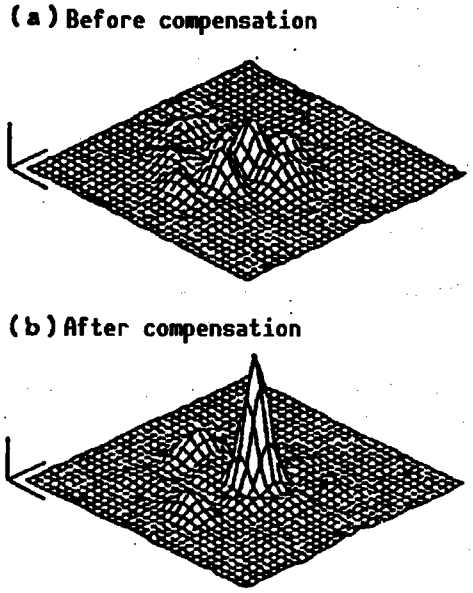

Figure 2. Beam Convergence Pattern at the Plane of the Convergence Point

Estimation of Sound Source Position by Modal Processing

93FE0340V Tokyo TECHNICAL RESEARCH AND DEVELOPMENT INSTITUTE, DEFENSE AGENCY in Japanese Nov 92 p 22

[Article by Yasunaga Toda and Kazuhiko Ota, staff members, 2nd Acoustic Research Office, Department 1, Fifth Research Center]

[Text] **1. Objective**

One method of estimating the distance and depth of a sound source from the signals received by the receiving equipment group arranged perpendicularly in the sea is the modal processing method which makes use of the normal mode propagation characteristics of the ocean. We have created a modal processing program and conducted simulation of sound source position estimation, and report the results here.

2. Methods Used and Content

Figure 1 is a process block diagram. Modal processing is a method that extracts sound source position information from a measured noise field, and estimates the position of the sound source by calculating the correlation of that information with values simulated by a sound wave propagation model. The marine sound field according to the sound source frequency component determined from the results of Fourier transform of the received signal was input to a mode filter, and the position information function was extracted. In addition, sound sources were placed in virtual positions, and the position information functions corresponding to each sound source were calculated. Correlations between these values and the position information functions

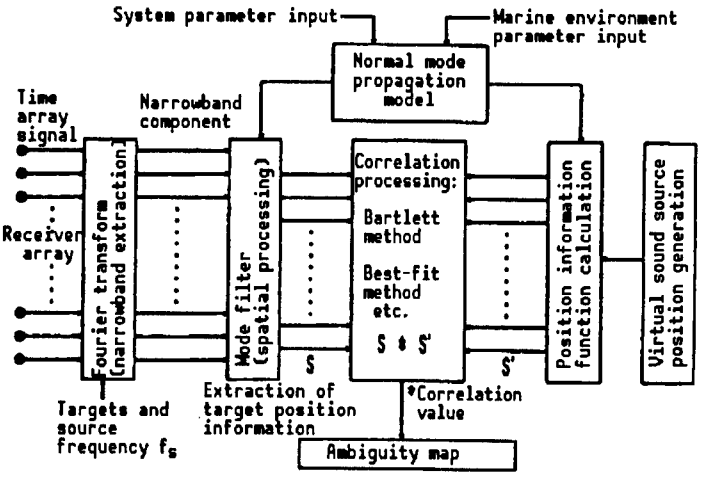

Figure 1. Process Block Diagram of Modal Processing

obtained from received signals were determined and drawn as an ambiguity map, and the sound source position was estimated. A normal mode propagation model was used in calculation of the mode filter coefficients and position information functions. In experimentation, a simulated sound field was used in place of received signals.

3. Results and Observations

(1) Results

Figure 2 [not reproduced] shows the results of sound source position estimation using a simulated sound field as input. The sound source position was 7,000 m distant and 20 m deep; the best fit method was used in correlation processing. The magnitude of the correlation value is shown in gray scale, with higher correlations shown by darker color. The result of the experiment was that the maximum value shown was the correlation value for the correct sound source position.

(2) Observations

White noise was included in the simulated sound field used, but clear estimation of the sound source position was possible; this method was shown to be appropriate. Further study of errors is to be carried out using actual marine data.

New Signal Processing Method in Lofargrams

93FE0340W Tokyo TECHNICAL RESEARCH AND DEVELOPMENT INSTITUTE, DEFENSE AGENCY in Japanese Nov 92 p 23

[Article by staff members Mamoru Egawa and Toshikazu Ohama of the 3rd Acoustic Research Office, Department 1, Fifth Research Center]

[Text] **1. Objective**

The detection and classification of target signals in passive sonar is done with lofargrams that present a time display of the results of frequency analysis. The conventional method of frequency analysis has been the fast Fourier transform (FFT) method, but because the width of the analysis is the reciprocal of the observation period in the FFT method, narrowing the analysis width lengthens the observation period, and it is difficult to detect signals with transitional sounds or fluctuations. Another problem is that spectra cannot be estimated accurately during analysis of very low frequency signals. Moreover, when the analysis width is narrow, noise is displayed continuously because of overlap processing (processing to overlap the observation periods), and the signal detection capability is reduced.

To solve the problems seen in the FFT method, we applied the instant covariance method to lofargrams, and compared the results with the FFT method.

2. Methods Used and Content

Under processing by the instant covariance method, if x(t) represents the data being processed, the instant covariance value $R_{ij}(t)$ is calculated by the formula

$$R_{ij}(t) = x(t-i) \cdot x(t-j) \tag{1}$$

and the forecast coefficient a_k is found with formula (2) below.

$$\begin{pmatrix} a_1 \\ a_2 \\ \vdots \\ a_m \end{pmatrix} = - \begin{pmatrix} R_{11} & R_{21} & \cdots & R_{m1} \\ R_{12} & R_{22} & \cdots & R_{m2} \\ \vdots & \vdots & \ddots & \vdots \\ R_{1m} & R_{2m} & \cdots & R_{mm} \end{pmatrix}^{-1} \begin{pmatrix} R_{01} \\ R_{02} \\ \vdots \\ R_{0m} \end{pmatrix} \tag{2}$$

By calculating the forecast coefficient a_k, the spectrum H(f) of a frequency f is found by formula (3) (where f_{max} is the maximum frequency).

$$|H(f)|^2 = 1/|1+\sum_{k=1}^{m} a_k \cdot \exp(-j\pi kf/f_{max})|^2$$

In experiments, frequency modulated signals, pulsed signals and square wave signals were added to noise, and the new method was compared with the FFT method in terms of ability to follow changes in frequency over time, ability to detect continuing signals, and ability to detect signals in relation to the signal to noise ratio.

3. Results and Observations

(1) Results

The figure [not reproduced] shows examples of lofargrams made with the instant covariance method and the FFT method. The results of experimentation confirmed that while the spectrum spread (analysis width) varies with the amount of data under the FFT method, it does not vary with the amount of data under the instant covariance method, and so the filter characteristics are extremely narrow. As a result, the detection capability is as good as that of the FFT method or better, even in the case of narrow-band analysis.

(2) Observations

The lofargrams confirmed that the instant covariance method had a superior detection capability for signals that were difficult to detect with the FFT method. It is thought that this method will improve the search and classification capabilities of passive sonar. Further theoretical study is to be given to signal detection capability hereafter.

Sound Absorption of Pine Wedges in Relation to Pressure

93FE0340X Tokyo TECHNICAL RESEARCH AND DEVELOPMENT INSTITUTE, DEFENSE AGENCY in Japanese Nov 92 p 24

[Article by Sanao Yamashita, Toshiaki Takahashi and Tomigo Yoroi, staff members, 3rd Aquatic Weapons Research Office, Bureau 2, Fifth Research Center]

[Text] **1. Objective**

Much research has been done on the sound-absorbing wedges used in air-filled anechoic chambers, and their properties have been made quite clear. On the other hand, pine wedges are generally used as sound-absorbing material in water-filled tanks, and their acoustic properties in relation to pressure are not well known.

A new, high-pressure anechoic tank has been set up in Department 2 of the Fifth Research Center to research, test and evaluate the pressure and acoustic properties of aquatic weapons. A study of the acoustic properties under pressure of pine wedges for absorption of sound in water (hereafter called "these wedges") is reported here.

2. Methods Used and Content

(1) Measurement of sound absorption by the reverberation time method

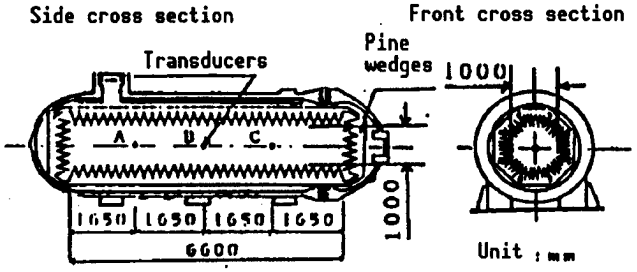

Figure 1. Overview of High-Pressure, Anechoic Water Tank

These wedges were placed in a high-pressure tank as shown in Figure 1. Band noise was generated using transducer A or B as the sound source; the sound source was cut off after reaching a steady state, and the remaining transducers measured the reverberation time until the sound pressure was attenuated to 60 dB. The results were averaged for calculation of the rate of sound absorption.

(2) Measurement of sound absorption by distance changes

As shown in Figure 2, burst waves (formed by modulating a sine wave with a square wave) were generated by transducer A and the sound pressure level was measured at various positions of transducer B, a movable underwater sensor.

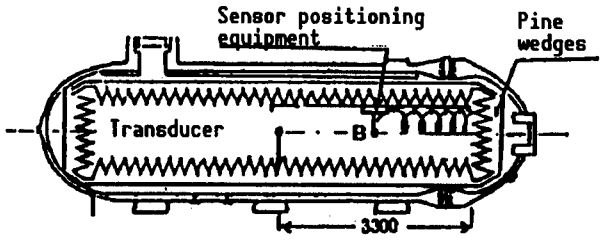

Figure 2. Measurement of Sound Pressure Level by Distance Changes

3. Results and Observations:

(1) Results

The results of sound absorption measurement by the reverberation time method are shown in Figure 3. Characteristics of sound pressure level attenuation with distance in relation to water pressure at a frequency of 40 kHz are shown in Figure 4.

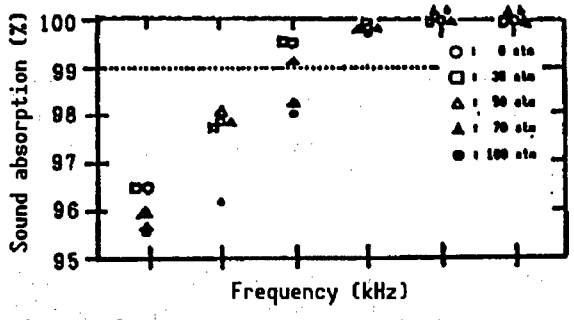

Figure 3. Results of Sound Absorption Measurement by the Reverberation Time Method

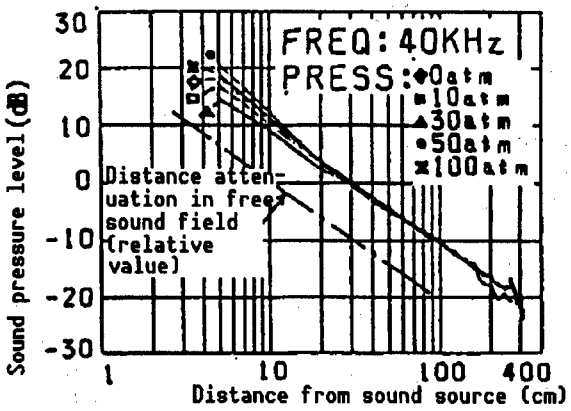

Figure 4. Sound Pressure Attenuation With Distance in Relation to Water Pressure

(2) Observations

a) Variation of sound absorption of these wedges in relation to water pressure can be ignored.

b) It was confirmed, as in Figure 3, that sound absorption by these wedges at about 16 kHz and above is 99% or more.

c) Near the central axis between these wedges, as shown in Figure 4, the sound pressure level is inversely proportional to the square of the distance from the sound source to a distance of 2 m; the formation of a free sound field was confirmed.

- END -

BULK RATE
U.S. POSTAGE
PAID
PERMIT NO. 352
MERRIFIELD, VA.
22161

NTIS
ATTN PROCESS 103
5285 PORT ROYAL RD
SPRINGFIELD VA

This is a U.S. Government publication. Its contents in no way represent the policies, views, or attitudes of the U.S. Government. Users of this publication may cite FBIS or JPRS provided they do so in a manner clearly identifying them as the secondary source.

Foreign Broadcast Information Service (FBIS) and Joint Publications Research Service (JPRS) publications contain political, military, economic, environmental, and sociological news, commentary, and other information, as well as scientific and technical data and reports. All information has been obtained from foreign radio and television broadcasts, news agency transmissions, newspapers, books, and periodicals. Items generally are processed from the first or best available sources. It should not be inferred that they have been disseminated only in the medium, in the language, or to the area indicated. Items from foreign language sources are translated; those from English-language sources are transcribed. Except for excluding certain diacritics, FBIS renders personal names and place-names in accordance with the romanization systems approved for U.S. Government publications by the U.S. Board of Geographic Names.

Headlines, editorial reports, and material enclosed in brackets [ ] are supplied by FBIS/JPRS. Processing indicators such as [Text] or [Excerpts] in the first line of each item indicate how the information was processed from the original. Unfamiliar names rendered phonetically are enclosed in parentheses. Words or names preceded by a question mark and enclosed in parentheses were not clear from the original source but have been supplied as appropriate to the context. Other unattributed parenthetical notes within the body of an item originate with the source. Times within items are as given by the source. Passages in boldface or italics are as published.

SUBSCRIPTION/PROCUREMENT INFORMATION

The FBIS DAILY REPORT contains current news and information and is published Monday through Friday in eight volumes: China, East Europe, Central Eurasia, East Asia, Near East & South Asia, Sub-Saharan Africa, Latin America, and West Europe. Supplements to the DAILY REPORTs may also be available periodically and will be distributed to regular DAILY REPORT subscribers. JPRS publications, which include approximately 50 regional, worldwide, and topical reports, generally contain less time-sensitive information and are published periodically.

Current DAILY REPORTs and JPRS publications are listed in *Government Reports Announcements* issued semimonthly by the National Technical Information Service (NTIS), 5285 Port Royal Road, Springfield, Virginia 22161 and the *Monthly Catalog of U.S. Government Publications* issued by the Superintendent of Documents, U.S. Government Printing Office, Washington, D.C. 20402.

The public may subscribe to either hardcover or microfiche versions of the DAILY REPORTs and JPRS publications through NTIS at the above address or by calling (703) 487-4630. Subscription rates will be provided by NTIS upon request. Subscriptions are available outside the United States from NTIS or appointed foreign dealers. New subscribers should expect a 30-day delay in receipt of the first issue.

U.S. Government offices may obtain subscriptions to the DAILY REPORTs or JPRS publications (hardcover or microfiche) at no charge through their sponsoring organizations. For additional information or assistance, call FBIS, (202) 338-6735,or write to P.O. Box 2604, Washington, D.C. 20013. Department of Defense consumers are required to submit requests through appropriate command validation channels to DIA, RTS-2C, Washington, D.C. 20301. (Telephone: (202) 373-3771, Autovon: 243-3771.)

Back issues or single copies of the DAILY REPORTs and JPRS publications are not available. Both the DAILY REPORTs and the JPRS publications are on file for public reference at the Library of Congress and at many Federal Depository Libraries. Reference copies may also be seen at many public and university libraries throughout the United States.